Published by Nigerian Society of Physical Sciences. Hosted by FLAYOO Publishing House LTD

Recent Advances in Natural Sciences

Journal Homepage: https://flayoophl.com/journals/index.php/rans

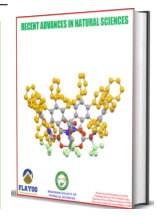

The correlation of geothermal energy potential deduced from aeromagnetic and aeroradiometric data of Akiri and anvirons, North-Central Nigeria

Bemsen Emmanuel Ikumbur*

Department of Geology, Benue State Polytechnic, Ugbokolo, Nigeria

ARTICLE INFO

Article history:
Received 18 July 2023
Received in final form 25 August 2023
Accepted 26 August 2023
Available online 28 August 2023

Keywords: Curie point depth, Geothermal heat, Radiometric heat, Spectral analysis, Geothermal gradient.

ABSTRACT

The aeromagnetic and aeroradiometric data were combined to investigate the geothermal energy potential of Akiri and Environs, North-Central Nigeria. The aeromagnetic and aeroradiometric data were obtained from the Nigerian Geological Survey Agency (NGSA), Abuja. The data consists of nine square map sheets of Wamba, Kwolla, Shendam, Lafia, Akiri, Ibi, Makurdi, Akwana and Wukari. The LANDSAT imagery data of the study area was obtained from the National Centre for Remote Sensing, Jos. The spectral analysis method was applied to aeromagnetic data to obtain the geothermal parameters of the magnetic sources. The results show that the depth-to-top of magnetic sources in the study area ranges between 0.76 and 4.46 km; while the depth-to-centroid ranges between 7.29 and 19.6 km. The depth-to-bottom of magnetic sources corresponds to the Curie point depth (CPD) in the study area which is the depth at which magnetic rocks lose their magnetism.. The results show that the CPD varies between 12.70 and 37.22 km, the geothermal gradient varies between 15.58 and 45.67°C/km, and the geothermal heat flow varies between 38.9 and 114.17mW/m^2. Two dimensional structural models were constructed to show the estimated depths at each profile taken. The models show uplifted crust and mantle in some areas due to magmatic intrusions which gave rise to low CPDs (12 to 28 km) which resulted to high geothermal heat flow values (60 to 115mW/m^2). The results show that there are low values of CPD in some areas which indicates that the study area has geothermal energy potential. The study shows that the geothermal energy potential deduced from aeromagnetic data correlates well with the geothermal energy potential deduced from aeroradiometric data.

1. INTRODUCTION

In recent years, combined aeromagnetic and radiometric surveys have been used as geological mapping tools and investigation of depths to magnetic sources. Aeromagnetic and radiometric data can be manipulated in a variety of ways, to minimize noise, enhance particular aspects of the data and integrate with other geosciences and geographic data, such as LANDSAT imagery data. Typically, the ultimate goal is to produce an interpretation focusing on one or more particular problems that provide a

*Corresponding author: Tel.: +234-813-622-0242;
e-mail: ibemsen@gmail.com (Bemsen Emmanuel Ikumbur)

reasonable and accurate depiction of geology. These problems include: geothermal exploration, research on radioactive heat, hydrocarbon survey, provision of the third dimension to surface mapping and sampling, delineation of structures, magnetic and radiometric minerals investigation using cost effective airborne measurements.

Geothermal energy has become a viable alternative and sustainable source of energy in many countries of the world. The energy is commonly manifested on the earth's surface in form of volcanoes and fumaroles (holes where volcanic gases are released), hot springs, steaming grounds and altered grounds [1]. The economically usable geothermal energy is that which occur close to the earth's surface where it can be tapped by drilling wells up to 3 km below the earth's surface. Such shallow heat sources are in most cases attributed to volcanic activity which are commonly associated with plate boundaries, and other geodynamic environments [1]. There is great need for renewable energy sources in Nigeria, such as the geothermal energy, since other energy sources like petroleum and gas are fast depleting. Hence there is pressing need for renewable energy in the country. This informs the decision to investigate the geothermal energy potentials in Nigeria.

In the present study, we shall investigate the geothermal energy potentials of Akiri and Environs using aeromagnetic and aeroradiometric data. The study area was chosen because of the evidence of hot springs in and near the study area. As Nigeria is one of the biggest producers of oil and gas in the world, hydrocarbons are the major source for general energy production.

The general problem within Nigerian energy sector is that the demand exceeds the energy generated. With a fast growing population, Nigeria needs an alternative renewable energy source, since the oil and gas reserves are fast depleting. Geothermal energy is preferred because it is an abundant, cost effective, secure, unpolluted and clean source of energy, which originated from the formation of the earth and from radioactive decay of elements within the basement complex rocks. Moreover, geothermal investigations have not received enough attention across Nigeria including the study area; as such there is missing gap in crustal temperature information.

The aim of this study is to investigate geothermal energy potentials of Akiri and Environs, North- Central Nigeria. The specific objectives are to: integrate the aeromagnetic and aeroradiometric; compare the radiometric heat and the geothermal heat flow to delineate areas with geothermal energy potentials in the study area.

The study area is located in the North Central part of Nigeria which comprises of the middle part of the Benue Trough of Nigeria and the Basement Complex. It is bounded by latitudes 7°30′N to 9°00′N and longitudes 8°30′E to 10°00′E (Figure 1). The Middle Benue Trough links the upper and lower arms of the Benue Trough sedimentary basin in Nigeria. It is part of the long stretch arm of the Central African Rift System and one of the seven inland sedimentary basins in Nigeria originating from the early Cretaceous rifting of the Central West African basement uplift [2]. The Benue Trough is a linear Northeast to Southwest (NE-SW) trending structure characterized by the presence of thick sedimentary cover of varied composition whose age ranges from Albian to Maastrichtian [2].

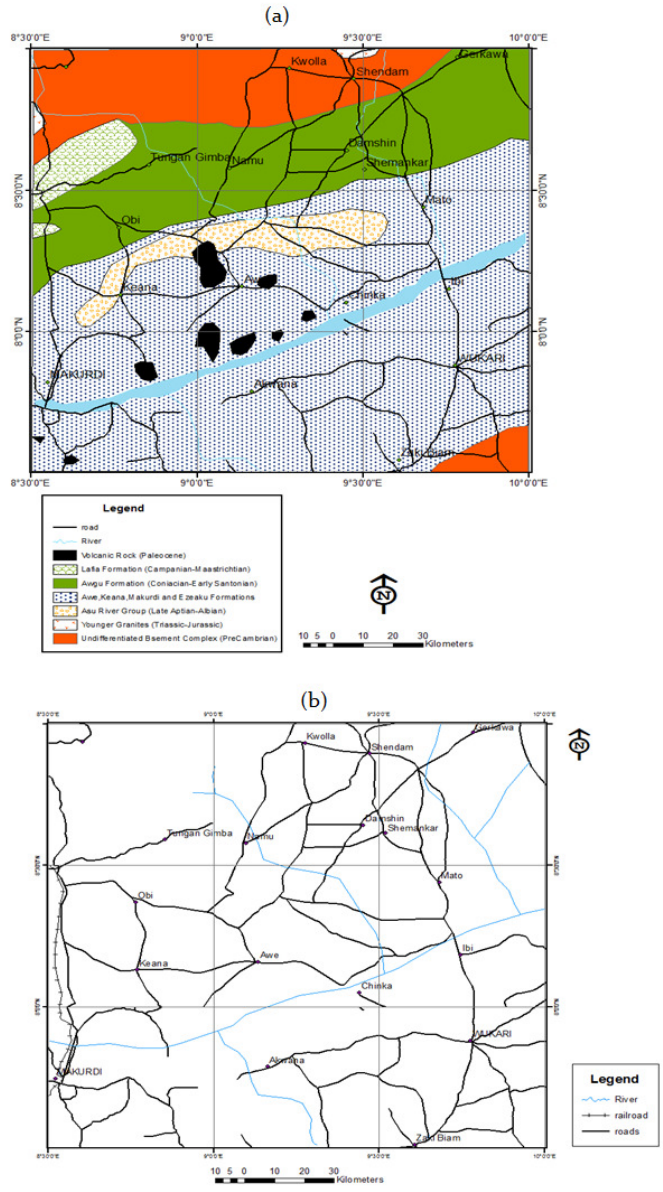

Fig. 1. (a) Geological map of the study area [5, 6]. (b) Location map of the study area.

The study area is underlain by the crystalline basement rocks, younger granites, sedimentary rocks and volcanic rocks [3–5]. Crystalline basement rocks of the Northern Nigerian Basement Complex underlie the northern and south-eastern parts of the study area, respectively (Figure 1. These crystalline basement rocks are grouped into two kinds, namely Migmatite-Gneiss Complex and the Older Granite.

2. MATERIALS AND METHODS

2.1. DATA ACQUISITION AND PROCESSING

Both the aeromagnetic and aeroradiometric data sets were obtained from the Nigerian Geological Survey Agency (NGSA) Abuja, in digitized form. The data sets are from the new high-resolution airborne survey coverage in Nigeria carried out by Fugro Airborne Surveys between 2006 and 2009 for the Nigerian

Geological Survey Agency. The aeromagnetic and radiometric surveys were flown along a series of NW-SE flight lines, spaced 500m, with 2000m tie-line spacing in a NE-SW direction and 80m nominal flight height. The data were recorded at 0.1 second interval. It consists of nine square map sheets of Wamba, Kwolla, Shendam, Lafia, Akiri, Ibi, Makurdi, Akwana and Wukari. Each square block represents a map on the scale of 1:100,000 and is (55×55) km^2 covering an area of 3,025 km^2, hence the study area is 27, 225 km^2.

The nine aeromagnetic maps covering the survey area were assembled to form a composite map which was re-contoured to produce the total magnetic intensity (TMI) anomaly map (Figure 2). The contouring was done using computer software (Surfer Version 32). Similarly, the nine aeroradiometric data sheets were re-contoured to produce one map for each of the three radiometric elements, potassium (K), thorium (Th) and Uranium (U) (Figures 9a, 9b and 9c respectively). From the heat calculations, a single radiometric heat map was produced (Figure 10).

The LANDSAT imagery map was obtained from the National Centre for Remote Sensing, Jos (Figure 5b). The data is part of the whole Satellite map of Nigeria acquired by Geomatics International Inc., for the Federal Department of Ministry of Agriculture and Natural Resources. It was selected from a main LANDSAT 5-TM (Thematic Mapper) Scene P188R54 covering the study area. The structural lineaments were mapped using ILWIS 3.3.The computer software SURFER 32 was used to construct the lineament map of the study area.

The contoured total magnetic intensity (TMI) map contains both the regional and residual anomaly. The regional gradient was removed from the map by fitting a linear surface to the aeromagnetic data using a multiple regression technique.

The surface linear equation on the data can be given according to [7] and [8] as;

$$p\,(x, y) = ax + by + c, \tag{1}$$

where, a, b and c are constants; x and y are distances in x and y axes. The $p(x, y)$ is the magnetic value at x and y co-ordinates. The Least squares method of statistical analysis was used to obtain the constants (a, b and c).

The trend surface equation was then subtracted from the aeromagnetic (observed) data and the resultant residual aeromagnetic anomaly data was obtained and contoured. After removing the trend, the remaining part of the time series consists of a signal (the periodic components) and noise (the random components)

2.2. ESTIMATION OF DEPTH TO MAGNETIC BASEMENT

Graphs of the natural logarithms of the main amplitude (A_n) against frequency (n) were plotted and the linear segments from the low frequency portion of the spectral were drawn from the graphs. The gradient of the linear segments were computed and the depths to the basement were determined using the equation according to [9], given as;

$$Z_t = -\frac{ML}{2\pi}, \tag{2}$$

where Z_t denotes the depth to the basement (depth to top), M is gradient of the linear segment, and L represents the length of the cross-section of the anomaly.

In the present study, the parameters needed are the depth-to-top of magnetic source, depth to centroid, depth to base of magnetic source which is known as Curie point depth. Curie point depth is the depth at which magnetic minerals lose their magnetism due to the effect of temperature (temperature range of 530°C to 580°C is taken as the Curie point temperature).

To obtain the depth to Curie point, spectral analysis of 2D Fourier transform of the aeromagnetic data was performed. To carry out spectral analysis, seven magnetic profiles were selected and used for detailed interpretation. The analysis was carried out using computer software Microsoft Excel Package.

To perform the analysis, the depth to centroid (Z_0) of the magnetic source from the slope of the longest wavelength part of the energy spectrum and the depth to the top (Z_t) of the magnetic source from the slope of the second longest wavelength part of spectral segment were estimated.). The depth to base (Z_b) of the magnetic source is calculated from the equation below, according to Refs. [10, 11].

$$Z_b = 2Z_0 - Z_t, \tag{3}$$

where Z_0 is the centroid depth (depth to centre of magnetic source), Z_t is the depth to top of magnetic source (sedimentary thickness) and Zb is the basal depth (depth to the bottom of magnetic source).

2.3. ESTIMATION OF HEAT FLOW AND GEOTHERMAL GRADIENT

To calculate the heat flow and geothermal gradient values we use the Fourier's law with the following formula, according to Tanaka *et al.* [12]:

$$Q = \frac{\lambda dT}{dz}, \tag{4}$$

where, Q is the geothermal heat flow and λ is the coefficient of thermal conductivity (given as 2.5 W/m°C). In this equation, it is assumed that the direction of the temperature variation is vertical and the temperature gradient dT/dz is constant as there is no heat gain or loss above the crust and below the Curie point depth. According to [12], the Curie temperature (θ_c) was obtained from the Curie point depth (Z_b) and the thermal gradient dT/dz using the following equation;

$$\theta_c = \frac{dT}{dz} Z_b. \tag{5}$$

Provided that there are no heat sources or heat sinks between the earth's surface and the Curie-point depth, the surface temperature is 0°C and dT/dz is constant. The Curie temperature (the temperature at which rocks lose their spontaneous magnetization) depends on magnetic mineralogy. In addition to the above, from equation (4) and (5), a relationship was determined between the Curie point depth (Z_b) and the heat flow (Q) as follows according to [12]:

$$Q = \frac{\theta_c}{Z_b}\lambda, \tag{6}$$

In this equation, the Curie point depth is inversely proportional to the heat flow [12, 13]. In this research, the Curie point temperature of 580°C and thermal conductivity of 2.5 Wm/ ^{0}C as an

average for igneous rocks was used as standard [14] in the study area. Equation (5) was utilized to compute the geothermal gradient of the region as the ratio of Curie temperature to Curie point depth.

According to Refs. [12, 15, 16], we have:

$$\frac{dT}{dZ} = \frac{\theta_c}{Z_b}, \tag{7}$$

where dT/dZ is geothermal gradient, Z_b is the basal depth and θ_c is the standard Curie point temperature of 580°C.

2.4. RADIOMETRIC DATA PROCESSING

Radioactive heat production from radiometric data is given according to [17], by the expression:

$$A\left(\frac{\mu W}{m3}\right) = \rho\,(0.0952Cu + 0.0256CTh + 0.0348Ck)\,, \tag{8}$$

where A = radiometric heat ($\mu W/m^3$), ρ = density of rock in kg/m^2 [18], C_u, C_{Th} and C_k are the concentrations of Uranium, Thorium and Potassium (in ppm for C_u and C_{Th}, and % for C_k) respectively.

The concentration of the three radiometric elements is read from the radiometric map covering the nine sheets adopted for magnetic data processing [19]. The value of the radiometric element's concentration and various rock densities are applied in equation (8) to compute the radioactive heat for the study area.

3. RESULTS AND DISCUSSION

3.1. QUALITATIVE INTERPRETATION

The Total Magnetic Intensity (TMI) map of the study area is shown in Figure 2a. The total magnetic field from the study area ranges from 7800 to 8240 nanotesla (nT). Higher values (shown in red) are found in the northern, north central, western, south western and southern parts of the study area; while lower magnetic intensity values (shown in blue) are found in the northwest, northeast, central and south-eastern regions.

The study area is characterized by closely spaced linear subparallel contours which suggest that faults or local fractured zones may possibly pass through such areas (Figures 2a and 2b). The general trending fabric of the TMI anomalies is northeast to southwest (SW- NE) direction. The residual magnetic field map (Figure 2b) shows a general trending fabric of NE to SW direction similar to those of the TMI map. The elliptical contour closures seen in the study area suggests the presence of magnetic bodies. These features represent geologic lineaments and their positions are indicated by lines drawn parallel to the elongation and through the centre of the anomalies represented in Figure 5.

The residual anomaly map shows that the contour lines are widely spaced in the NW, West and SW parts of the study area, this indicates that there are thicker sediments in those regions (Wamba, Lafia, and Makurdi), implying that the depth to basement is deeper in these areas compared to the areas where there are closely spaced contours which suggests shallow sedimentary thickness.

Upward continuation is a method used to separate regional magnetic anomaly resulting from deep sources from the observed magnetic anomaly data. Upward continuation was applied to suppress the effects of small scale features near the surface and

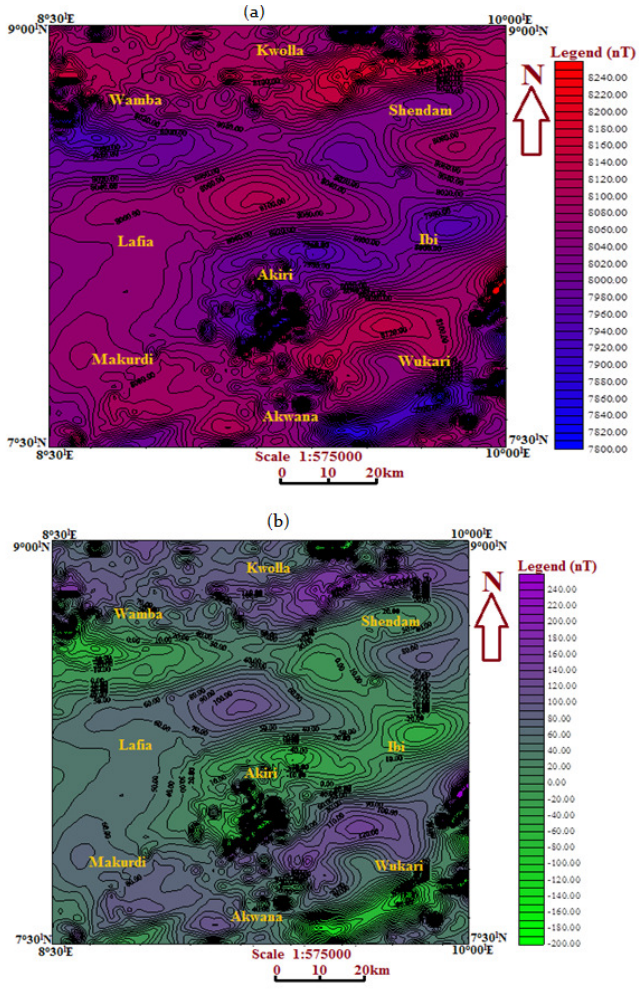

Fig. 2. (a) TMI Map of the Study Area (Contour Interval = 10 nT) (b) Residual Anomaly Map of the Study Area (Contour Interval = 10 nT.

also to reduce topographic effects. The upward continuation map of the study area (Figure 3a) shows areas with highest magnetic intensity in blue colour (near Kwolla). Wamba (North), Lafia, Makurdi and Akwana have higher intensity (red colour), while Akiri, Ibi, Wukari and Wamba (South) have lowest intensities (yellow colour).

Figure 3b shows the LANDSAT Imagery map of the study area which depicts the remotely sensed data of the area; these include detecting and monitoring the physical characteristics of the area in question by measuring its reflected and emitted radiation at a distance (typically from satellite or aircraft). These data can be used to interpret changes on and inside the earth such as temperate changes, images of the ocean floor, tracking clouds to help predict the weather or watching erupting volcanoes and mapping of the rugged topography of the earth. The lineaments identified and delineated on the study area are more concentrated on the Basement rocks than Younger Granites and Cretaceous Sedimentary rocks. This is due to the effects of the widespread Pan-African Orogeny that was experienced in the Nigerian Basement rocks. Figures 3(a), 3(b) and 4 show that the main trend of the lineaments is NE-SW, while minor ones trend E-W and NNE-SSW

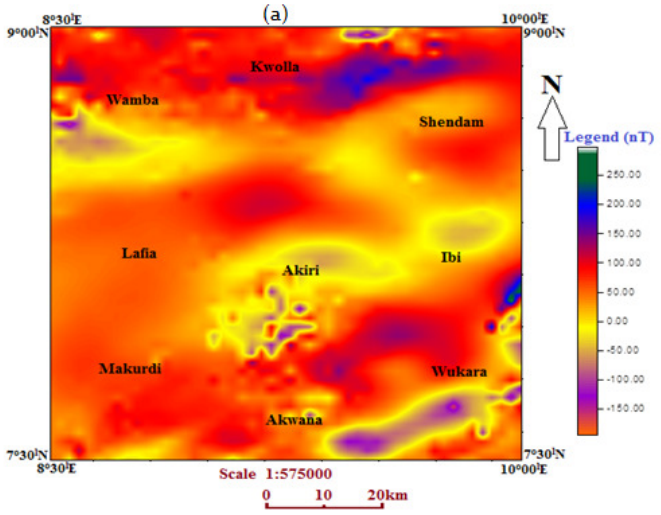

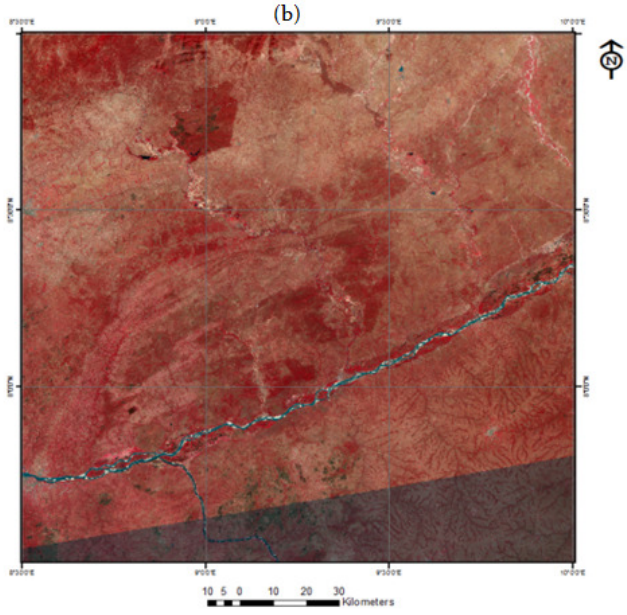

Fig. 3. (a) Upward Continuation Map of the Study Area. (b) LANDSAT Imagery Map of the Study Area.

directions. The major anticline identified on the map coincide with the Keana Anticline, trends NE-SW and extends from north-east of Makurdi via north of Keana to the north of Awe (Akiri). Three minor anticlines close to the major one with axis trending NE-SW also occurs. The main structural trends (NE-SW and E-W) agree with the magnetic trend results.

3.2. QUANTITATIVE INTERPRETATION

Seven profile lines, namely AA-GG^{l} were taken in the northwest-southeast (NW-SE) direction, and used for detailed interpretation (Figure 5). Using the Microsoft Excel package, the graphs of magnetic intensity against distance on the profiles were drawn to show the nature of magnetic anomalies found in the study area (Figure 6).

Spectral graphs were then obtained from the profiles by plotting the values of magnetic intensity against frequencies. These

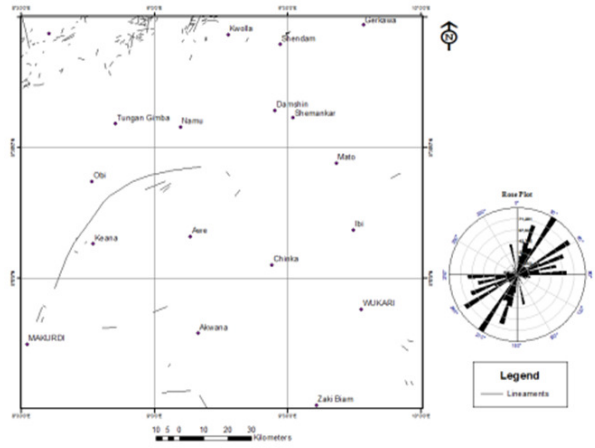

Fig. 4. Structural Lineament Map of the Study Area with Rose Diagram.

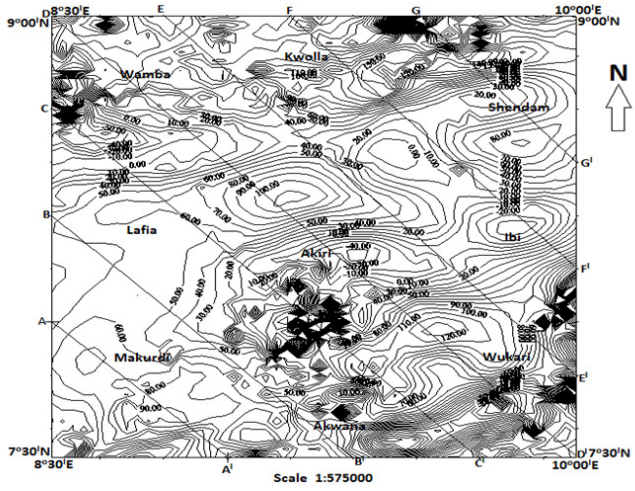

Fig. 5. Residual anomaly map of study area showing the profile lines.

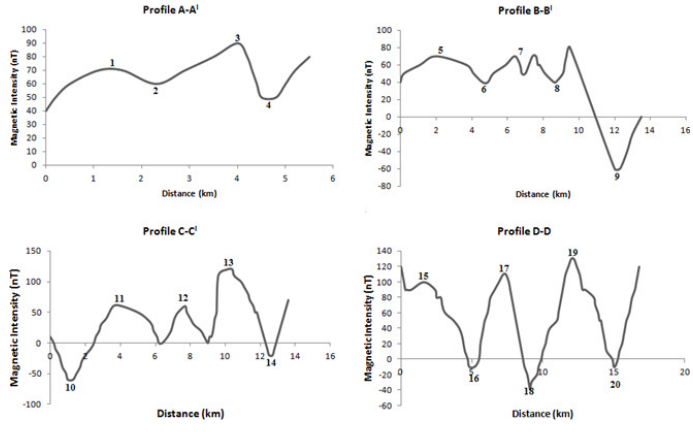

Fig. 6. Magnetic anomaly graphs shown on profiles A-A^{l} to D-D^{l}.

are graphs of the natural logarithms of the amplitudes against frequencies obtained for various profiles (A-A^{l} to G-G^{l}). Each graph has two line segments: the first line segment gives the depth-to-centroid (Z_0) representing depths to deeper sources, while the second line segment gives the depth-to-top of magnetic

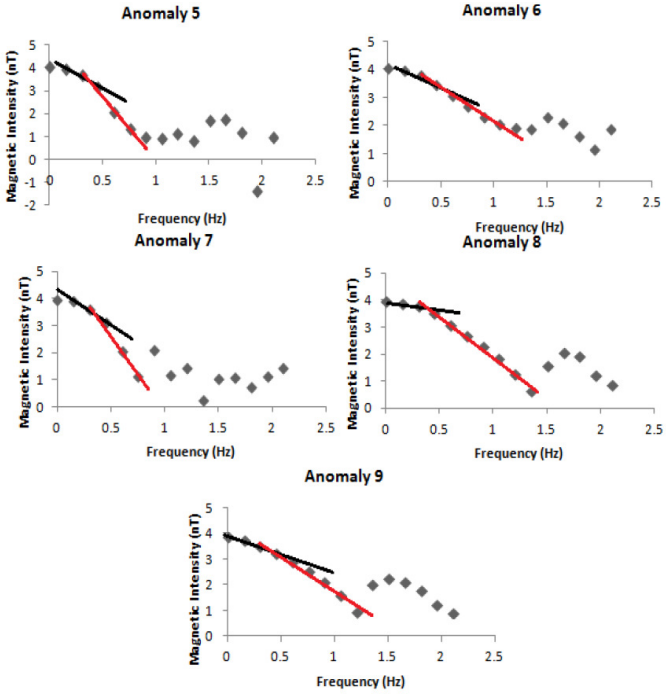

Fig. 7. Pectral graphs of profile A-A^{l}and B-B^{l}

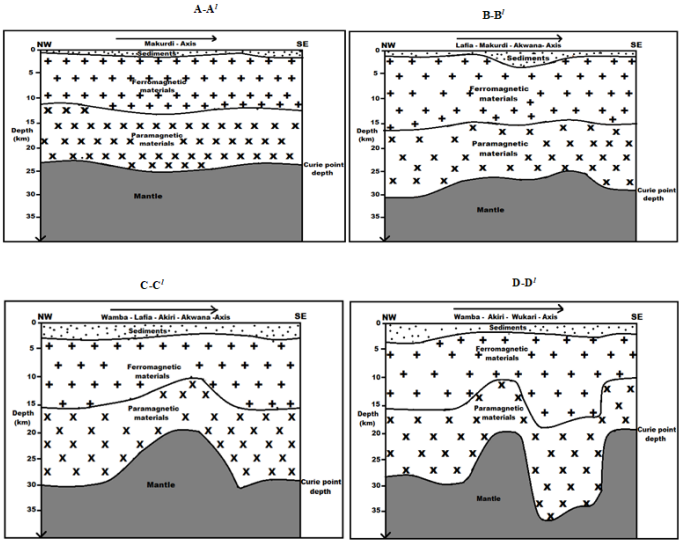

Fig. 8. Structural modelling along Profile A^{l}-A^{l} to D-D^{l} within the study area.

sources which shows shallower depths to magnetic sources. The gradient of the linear segments were calculated and the depth to magnetic sources (Z_0 and Z_t) were determined (Figure 7).

3.3. INTERPRETATION OF THE SPECTRAL GRAPHS AND STRUCTURAL MODELS

Each spectral graph has two line segments: the first line segment gives the depth-to-centroid (Zo) which is obtained by fitting a straight line through the low wave number part of the radially averaged power spectrum (RAPS), while the second line segment gives the depth-to-top of magnetic sources.

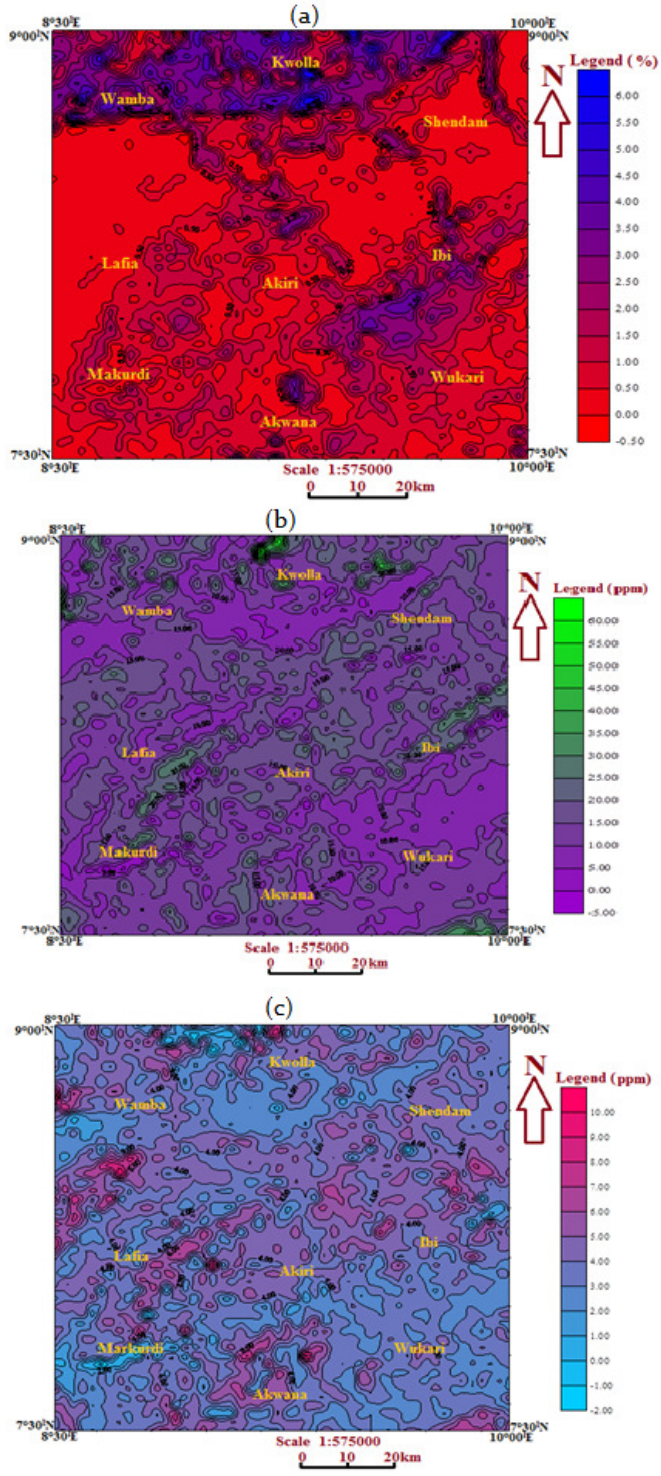

Fig. 9. (a) Potassium Data Map of the Study Area (contour Interval≈0.5%) (b)Thorium Data map for the Study Area (contour Interval≈5.0ppm) (c) Uranium Data map for the Study Area (contour Interval≈1.0ppm).

2D structural models were constructed to show the calculated depths (depth-to-top or sedimentary thickness, depth-to-bottom or Curie point depth) and estimated depth to Mantle plume.

Table 1. Estimated Curie point depths and geothermal parameters obtained from spectral analysis

Profile Name	Profile Location	Anomaly	Depth to Top (km)	Centroid Depth (km)	Curie Point Depth (km)	Geothermal gradient (^{0}C/km)	Heat Flow (mW/m^2)	Radiometric Heat ($\mu W/m^3$)
A-A′	Makurdi Axis	1	1.34	12.21	23.08	25.1230	62.8250	1.3466
		2	1.72	13.76	25.80	22.4806	56.2016	1.4151
		3	1.27	13.09	24.91	23.2838	58.2096	1.6432
		4	1.73	12.89	24.05	24.1164	60.2911	1.7474
B-B′	Lafia-Makurdi -Akwana	5	2.41	16.51	30.61	18.9481	47.3701	2.2341
		6	1.51	14.49	27.47	21.1139	52.7849	2.3064
		7	4.46	16.38	28.30	20.4947	51.2368	2.4415
		8	2.16	13.51	24.86	23.3307	58.3266	2.2957
		9	2.32	15.67	29.02	19.9862	49.9655	2.5547
C-C′	Wamba-Lafia -Akiri-Akwana	10	2.49	16.31	30.13	19.2499	48.1248	2.0605
		11	2.80	14.12	25.44	22.7987	56.9969	1.8994
		12	2.08	10.92	19.76	29.3522	73.3806	1.9742
		13	1.54	15.87	30.20	19.2053	48.0133	1.2730
		14	3.09	15.85	28.61	20.2726	50.6816	1.2623
D-D′	Wamba-Akiri -Wukari	15	3.62	15.76	27.90	20.7885	51.9713	1.3984
		16	2.30	16.18	30.06	19.2947	48.2369	1.4312
		17	2.27	11.31	20.35	28.5012	71.2531	1.6747
		18	1.98	19.60	37.22	15.5830	38.9576	1.7224
		19	2.57	18.11	33.65	17.2363	43.0906	2.1448
		20	2.14	11.27	20.40	28.4314	71.0784	2.1297
E-E′	Wamba/ Kwolla-Akiri -Wukari	21	2.57	12.62	22.67	25.5845	63.9612	1.8973
		22	2.28	19.24	36.20	16.0221	40.0553	1.8276
		23	2.14	17.38	32.62	17.7805	44.4513	1.7945
		24	1.91	18.41	34.91	16.6142	41.5354	1.5559
		25	1.73	17.76	33.79	17.1648	42.9121	1.8143
F-F′	Kwolla- Shendam-Ibi Axis	26	1.94	10.21	18.48	31.3853	78.4632	2.1630
		27	1.72	18.27	34.82	16.6571	41.6427	2.2121
		28	2.11	11.34	20.57	28.1964	70.4910	1.9483
		29	2.31	9.29	16.27	35.6484	89.1211	1.9630
		30	2.18	18.75	35.32	16.4213	41.0532	2.0028
		31	1.88	7.29	12.70	45.6693	114.1732	1.9248
G-G′	Shendam Axis	32	1.08	12.39	23.70	24.4726	61.1814	2.0491
		33	0.76	11.18	21.60	26.8519	67.1296	1.5892
		34	2.27	9.36	16.45	35.2584	88.1459	1.3975
		35	2.19	10.19	18.19	31.8857	79.7141	1.3483
Average			2.14	14.21	26.29	23.5772	58.9436	1.8412

The structural models show the sedimentary thickness, magnetic crust which hosts the Ferromagnetic materials and Paramagnetic materials, and the Mantle (Figure 8). The Ferromagnetic materials have high magnetic susceptibility, while the Paramagnetic materials have low magnetic susceptibility. In the Mantle, there are no magnetic materials because they lost their magnetic properties due to high temperature.

In Profile A-A^l(along Makurdi axis), the Curie Point Depth (CPD) is high due to deeper depth of Mantle Plume, because there is no evidence of uplift. This gives rise to lower values of geothermal heat flow (Figure 8 & Table 1).

In Profile B-B^l (along Lafia-Makurdi-Akwana axis), the CPD is high and the corresponding values of geothermal heat flow are low (Figure 8 & Table 1).

There is evidence of uplift in the middle of profile C- C^l which lies on Wamba-Lafia-Akiri-Akwana Axis. The uplift gives rise to low CPD and causes high geothermal heat flow (Figure 8 & Table 1).

Along Profile D-D^l (Wamba-Akiri-Wukari Axis), there are uplifts which give rise to low Curie Point Depth and these causes high geothermal heat flow in the area (Figure 8 & Table 1).

3.4. CURIE POINT DEPTH AND GEOTHERMAL PARAMETERS

Table 1 shows the estimated Curie point depths and geothermal parameters obtained from spectral analysis. Apart from the Curie point depth (Z_b), the geothermal parameters include: depth-to-top (Z_t) which ranges from 0.76 and 4.46 km, depth-to-centroid (Z_0) of magnetic source ranges from 7.29 and 19.60 km. The

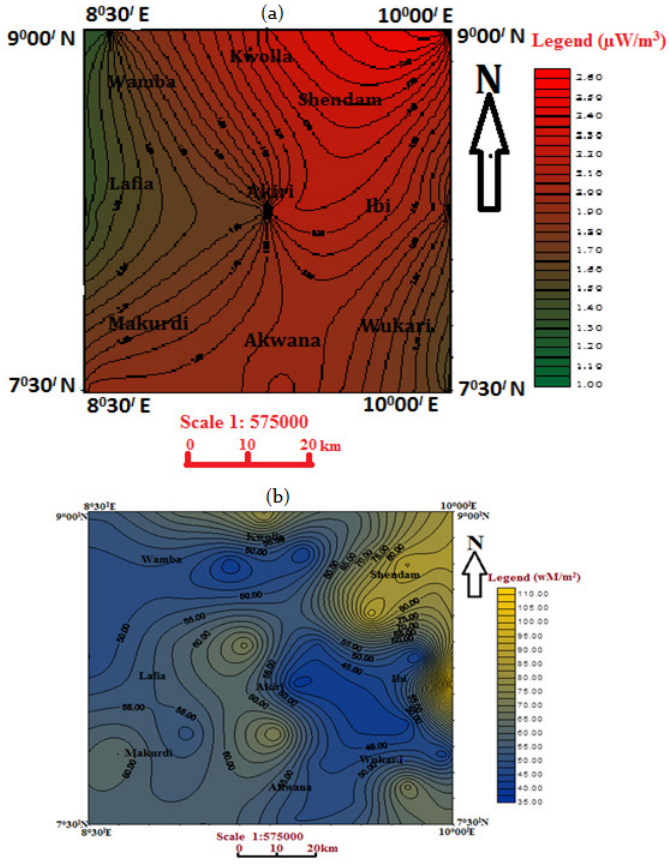

Fig. 10. (a) Radiometric Heat Map of the Study Area (Contour Interval ≈ 0.05 /m^3). (b) Heat Flow Map of the Study Area constructed from Aeromagnetic Data (Contour interval 1.0 wM/m^2).

Curie point depth of magnetic sources range from 12.70 to 37.22 km. The geothermal gradient (dT/dZ) varies from 15.58 to 45.67 °C/km, with an average of 23.58 °C/km. and geothermal heat flow (Q) values in the study area range from 38.958 to 114.173 mW/m^2. The average heat flow in the area is 58.94 mW/m^2.

The depths to top of magnetic sources represent shallower depths in the study area; while the depths to centroid of magnetic sources represent the depths to deeper sources. Curie point depth is the same as the average depth to bottom of magnetic source in the study area (26.29 km). The lowest geothermal gradient value corresponds to the lowest heat flow value, while the highest value corresponds to the highest heat flow value. The results obtained were used to construct the maps of depth-to-top (Z_t) and depth-to-centroid (Z_0) of magnetic sources in the study area.

3.5. RADIOMETRIC INTERPRETATION

Potassium (K) content map: Figure 9(a) is the Potassium content map of the study area. The map shows high concentration of potassium (K) around Wamba, Kwolla and part of Shendam (in the Northern part of the study area), between Ibi and Wukari, and Akwana. Low concentration of Potassium is prevalent around Lafia, Makurdi, part of Shendam, Akiri and part of Wukari. Shales, Sandstones and Granite are rocks associated with high potassium activity.

Thorium (Th) content map: Figure 9(b) is the Thorium content map of the study area. The map shows high concentration of Thorium around Wamba, Kwolla, Shendam, Lafia, Akiri, Ibi and Wukari south. Low concentrations of Thorium are predominant around Makurdi, Akwana, Akiri and Wukari. Mineralization associated with thorium includes basement granitic rocks, migmatite, shales and clay.

Uranium (U) content map: Figure 9(c) is the Uranium content map of the study area. The map shows high concentration of Uranium around Lafia, Akiri, Ibi, Akwana, south of Wukari and Makurdi north. Low concentration of U is found around Kwolla, Shendam, Wamba, Wukari and Makurdi south. Shales, clay and basement complex rocks are associated with uranium mineralization.

3.6. RADIOMETRIC HEAT MAP

High concentration of radiometric heat has the highest occurrence around Wamba, Kwolla, Shendam, Akiri, Ibi, Makurdi and Akwana (Figure 10(a)). These areas are the hot spots which are potential geothermal areas. Low concentrations are found around Wamba south, Kwolla south, Lafia, Shendam north and Wukari north (Figure 10(a)). The areas of high radiometric heat concentration correspond with the areas with low Curie point depth, high geothermal gradient and high geothermal heat flow (Figures 10a and 10(b)).

3.7. CORRELATION OF GEOTHERMAL ENERGY POTENTIAL DEDUCED FROM AEROMAGNETIC DATA AND AERORADIOMETRIC DATA OF THE STUDY AREA

From the study, areas around Kwolla, Shendam, Lafia, Akiri, Ibi, Makurdi and Akwana have high geothermal energy potentials, which is almost the same for both aeromagnetic interpretation and aeroradiometric interpretation in the study area (Figures 11(a) and 12(b)). The study shows that the geothermal energy potential deduced from aeromagnetic data correlates well with the geothermal energy potential deduced from radiometric data (Figure 11(a) and 12(b).

4. CONCLUSION

Based on the results obtained, the areas with high concentration of radiometric heat, low Curie point depth; high geothermal gradient and high geothermal heat flow are the hot spots for geothermal energy potential in the study area. Geologically, these areas are those covered by basement complex, volcanic intrusives; and sandstones and shales (in the sedimentary area). The aeromagnetic data was analysed through spectral method to obtain depths to top, depths to centroid, and depths to bottom of the magnetic sources. The depths to top of magnetic sources indicate the sedimentary thickness in the study area which ranges from 0.76 to 4.46 km, with an average of 2.14 km. Based on these thicknesses range, there is an indication that the possibility of hydrocarbon generation is feasible in the study area if all other conditions for hydrocarbon accumulation are favourable. I am thankful to Nigerian Geological Survey Agency (NGSA), Abuja, for the aeromagnetic and aeroradiometric data provided to me to aid in carrying out this research. I also appreciate the National Remote Sensing Centre, Jos, Nigeria.

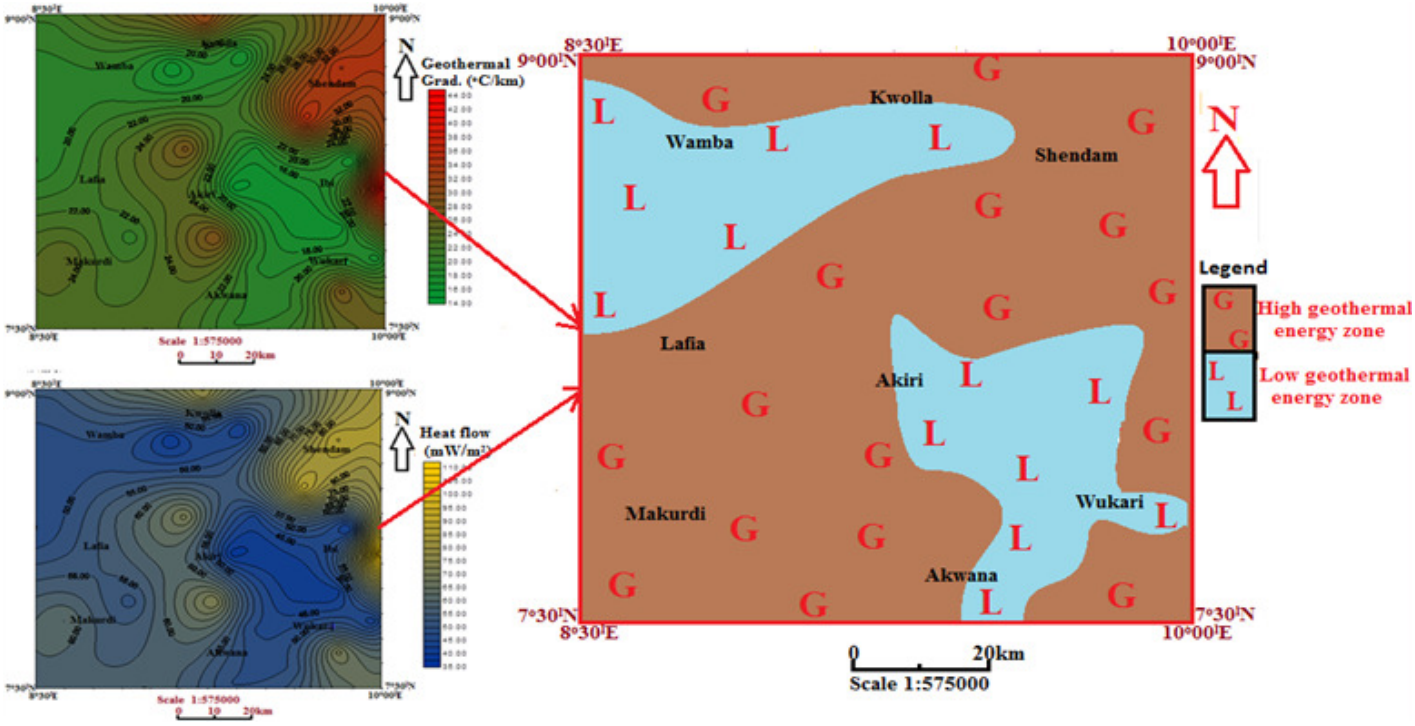

Fig. 11. A Geothermal Energy Potential map Deduced from Aeromagnetic Interpretation across the Study Area.

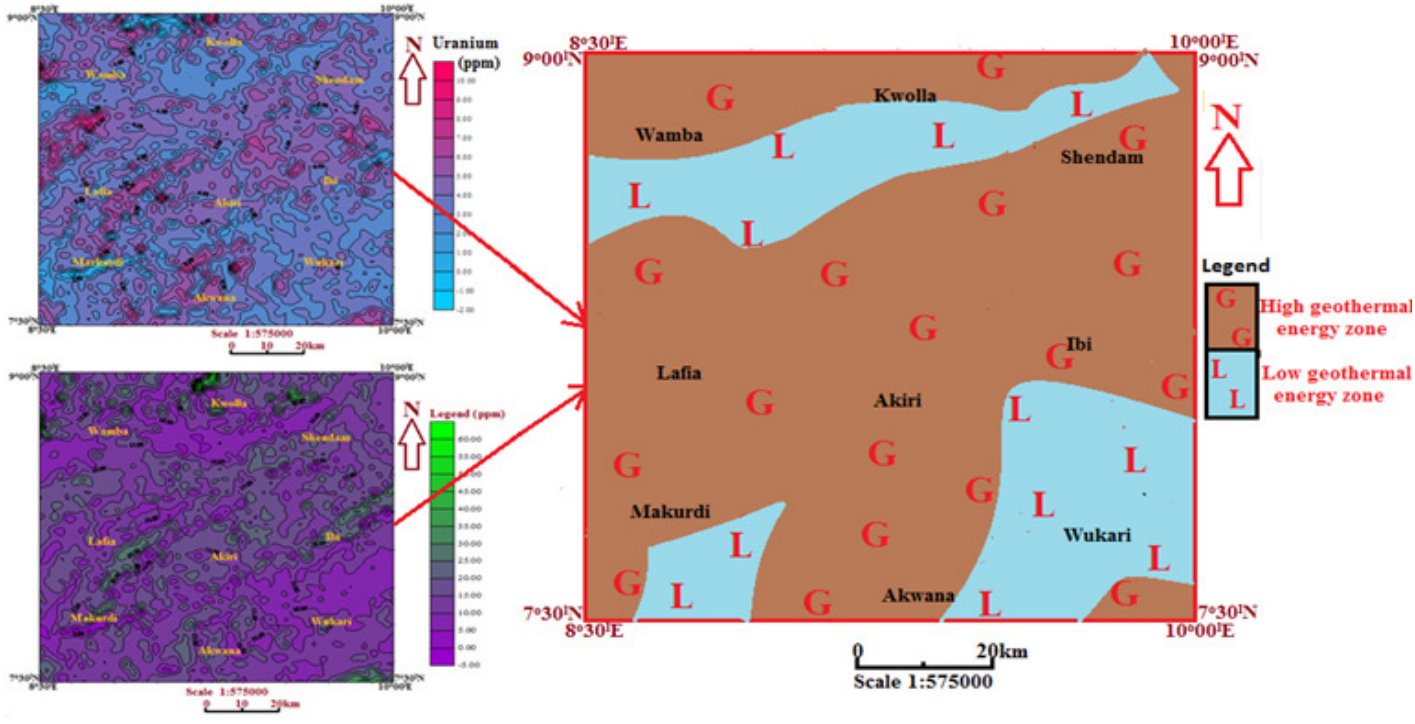

Fig. 12. A geothermal energy potential map deduced from aeroradiometric interpretation across the study area

The study has shown several new things derived from aeromagnetic and radiometric methods which in the past have not been adequately utilized.

- Correlation of the data sets used: The data sets (aeromagnetic, radiometric and LANDSAT imagery) used in the study area to investigate geothermal energy potential correlates well.
- Prediction of radiometric heat from geothermal heat: In the study, the higher the geothermal heat in the area, the higher the radiometric heat.
- Origin and Source of heat: The presence of magmatic intrusions in the crust, uplifted crust and mantle, major faults,

volcanic rocks, and high concentration of radiometric elements of K, Th, and U establishes the origin and source of heat in the study area.

- High geothermal energy: the study shows high subsurface heat flow and high concentration of radiometric heat in the study area.

The following recommendations are made for further studies based on the results obtained from the analyses of both the aeromagnetic and aeroradiometric data.

1. The spectral and radiometric heat production methods used in this study should be applied in other areas observed to have geothermal energy potential across Nigeria.
2. The geothermal parameters should be further investigated by carrying out borehole temperature logging in the study area.
3. In areas where there is high geothermal heat flow and high radiometric heat concentration (around Kwolla, Shendam, Lafia, Akiri, Ibi, Makurdi and Akwana), exploratory wells should be drilled to confirm the depths to heat sources.

References

[1] L. Ochieng, *Overview of geothermal surface exploration methods*, presented at *Short course VIII on exploration for geothermal resources*, organised by UNU-GTP, GDC and Ken-Gen, at lake Naivasha, Kenya October 31st - November 22nd, 2013. https://www.grocentre.is/gtp/moya/page/sc-21.

[2] N. G. Obaje, H. Wehner, H. Hamza & G. Scheeder, ‘‘New Geothermal data from the Nigerian sector of the Chad Basin: Implications on hydrocarbon Prospectivity", Journal of African Earth Sciences **38** (2004) 477. https://doi.org/10.1016/j.jafrearsci.2004.03.003

[3] M. E. Offodile, *A Review of the geology of the Cretaceous of the Benue Valley* In: *Kogbe, C.A. (Ed), Geology of Nigeria (Second Revised Edition)*, Rock View Nigeria Limited, Jos, 1989, pp. 538.

[4] N. G. Obaje, *Geology and Mineral Resources of Nigeria*, Lecture Notes in Earth Sciences, Springer, Berlin Heidelberg, 2009. https://doi.org/10.1007/978-3-540-92685-6.

[5] Nigerian Geological Survey of Agency, *Geology of the Benue Trough*, 2009.

[6] G. K. Anudu, R. A. Stephenson & D. I. M. Macdonald, *Using high-resolution aeromagnetic data to recognize and map intra-sedimentary volcanic rocks and geological structures across the Cretaceous Middle Benue Trough, Nigeria*, Journal of African Earth Sciences **99** (2014) 625. https://doi.org/10.1016/j.jafrearsci.2014.02.017

[7] O. K. Likkason, ‘‘Application of trend surface analysis of gravity data over the Middle Niger Basin, Nigeria", Journal of Mining and Geology **29** (1993) 11. https://nmgs-journal.org/wp-content/uploads/journal/published_paper/volume-29/issue-2/VP3Viyfp.pdf.

[8] J. C. Davis, *Statistics and Data Analysis in Geology*, John Wiley and Sons, New Delhi, India, 1972, pp. 638.

[9] J. G. Negi, P. K. Agrawal and K. N. N. Rao, ‘‘Three-dimensional model of the Koyan area of Maharshaitra State, India, based on the spectral analysis of aeromagnetic data", Geophysics **48** (1983) 964. https://doi.org/10.1190/1.1441522.

[10] Y. Okubo, R. G., Graff, R. O. Hansen, K. Ogawa & H. Tsu, ‘‘Curie point depths of the Island of Kyushu and Surrounding areas", Geophysics **53** (1985) 481. https://doi.org/10.1190/1.1441926.

[11] R. Bello, C.C. Ofoha & N. Wehiuzo, ‘‘Geothermal gradient, Curie point depth and heat flow determination of some parts of lower Benue Trough and Anambra basin, Nigeria, using high resolution aeromagnetic data, Physical Science International Journal **15** (2017) 1. https://doi.org/10.9734/PSIJ/2017/34654.

[12] A. Y. Tanaka, Y. Okubo & O. Matsubayashi, ‘‘Curie point depth based on spectrum analysis of the magnetic anomaly data in East and Southeast Asia", Tectonophysics **396** (1999) 461. https://doi.org/10.1016/S0040-1951(99)00072-4.

[13] A. Stampolidis, I. Kane, G. N. Tsokas& P. Tsourlos, ‘‘Curie point depths of Albania inferred from ground total field magnetic data", Surveys in Geophysics **26** (2005) 461. https://doi.org/10.1007/s10712-005-7886-2.

[14] L. I. Nwankwo, P. I. Olasehinde & C. O. Akoshile, Heat flow anomalies from the Spectral analysis of Airborne Magnetic data of Nupe Basin, Nigeria, Asian Journal of Earth Sciences **1** (2011) 1. https://scialert.net/abstract/?doi=ajes.2011.20.28.

[15] L. I. Nwankwo and A. T. Shehu, Evaluation of Curie-point depths, geothermal gradients and Near-surface heat flow from high-resolution aeromagnetic (HRAM) data of the entire Sokoto Basin, Nigeria, Journal of Volcanology, Geothermal Research **305** (2015) 45. https://doi.org/10.1016/j.jvolgeores.2015.09.017.

[16] H. E. Ross, R. J. Blakely & M. D. Zoback, ‘‘Testing the use of aeromagnetic data for the Determination of Curie depth in California", *Geophysics* 71 (2006) 51. https://doi.org/10.1190/1.2335572.

[17] A. Salem & D. Fairhead, ‘‘Geothermal reconnaissance of Gebel Dui area, Northern Red Sea, Egypt, using airborne magnetic and spectral data", GTECH (2011) 1.

[18] W. M. Telford, I. P. Geldart & R. E. Sheriff, *Applied Geophysics*, Second Edition, Springer, Berlin, 1990, pp 770.

[19] D. Beamish and J. Busby, ‘‘The Corrubian geothermal province: Heat production and flow in South-Western England: estimates from boreholes and airborne gamma-ray measurements", Geothermal Energy **4** (2016) 1.